ANALYSIS OF FIELD-SCALE SALINIZATION: A COMPARISON OF DIFFERENT MODELING APPROACHES

P. J. VAUGHAN[1)], P.J. SHOUSE[1)], D.L. SUAREZ[1)], M. TH. VAN GENUCHTEN[1*)] and J.E. AYARS[2)]

[1)]George E. Brown, Jr. Salinity Laboratory, USDA-ARS, 450 W. Big Springs Road, Riverside, CA 92507, USA;
mailto: rvang@ussl.ars.usda.gov
[2)]Water Management Research Laboratory, USDA-ARS, 9611 S. Riverbend Ave., Parlier, CA 93648, USA.

Soil and groundwater salinization are major problems for irrigated agriculture in many arid and semiarid areas of the world. Studies addressing such problems require accurate estimation of salt loadings from irrigated areas through the vadose zone to underlying groundwater. We studied Cl^- transport in the vadose zone at 45 locations in a field in the San Joaquin Valley, California, through a combination of soil sampling at six depths (0–1.8 m) and numerical modeling using a coupled water flow and solute transport code (Unsatchem). Our purpose was to assess water and salt loadings from the heterogeneous field to groundwater over a two-year period, and to test applicability of the code to the data. Soil sampling in November, 1995, defined the initial water content and the Cl^- concentration, and the soil hydraulic properties. Four more sampling periods, ending in November 1997, provided data for evaluating model performance. Cl^- distributions in 1997 exhibited a variety of shapes including monotonically increasing or decreasing distributions versus depth, and profiles with maxima, minima or and sigmoidal shapes. The standard modeling approach, based on the Richards equation and the convection-dispersion equation, predicted more Cl^- leaching than was observed in the field. Somewhat improved predictions were obtained when the potential transpiration rate was increased by a factor of 1.5. Better leaching predictions were also obtained when the model included separate mobile and immobile water fractions, mostly by improving the profile shapes. Our study shows the importance of accurate descriptions of the lower boundary conditions, spatial variability in the water infiltration rate, and estimation of soil surface evaporation and transpiration rates.

KEY WORDS: Solute Transport, Field Simulation, Chloride, Unsatchem.

P. J. Vaughan, P.J. Shouse, D.L. Suarez, M. Th. van Genuchten, J.E. Ayars: ANALÝZA ZASOLENIA V MIERKE POĽA: POROVNANIE ROZDIELNYCH MODELOVÝCH PRÍSTUPOV. Vodohosp. Čas., *53*, 2005, 2; 40 lit., 9 obr., 3 tab.

Zasoľovanie pôdy a podzemných vôd sú hlavnými problémami pôdohospodárstva v závlahových podmienkach v mnohých aridných a semiarídnych oblastiach sveta. Štúdie, ktoré riešia podobné problémy, vyžadujú si presné určenie zaťaženia soľami zo závlah, ktoré prechádzajú nenasýtenou oblasťou pôdy do podzemných vôd. V tejto štúdii sa zaoberáme transportom Cl^- v nenasýtenej oblasti pôdy v 45 lokalitách v San Joaquin Valley, California, využívajúc kombináciu odberu vzoriek pôdy v šiestich hĺbkach (0–1.8 m) a numericakým modelovaním s využitím simulačného modelu kombinovaného transportu vody a rozpustených látok (solí) (Unsatchem). Cieľom je určenie priesaku vody a rozpustených látok z heterogénneho poľa do podzemných vôd počas dvojročného obdobia a testovanie použiteľnosti uvedeného modelu vzhľadom k vstupným hodnotám. Zo vzoriek pôdy, odobratých v novembri 1995 bolo určené počiatočné rozdelenie vlhkosti pôdy a koncentrácia Cl^-, ako aj hydraulické vlastnosti pôdy. Štyri ďalšie termíny odberov, končiac v novembri 1997, poskytli údaje pre overenie modelu. Rozdelenie Cl^- v roku 1997 sa vyznačovalo rozdieľnosťou tvarov, vrátane monotónne klesajúceho alebo stúpajúceho rozdelenia koncentrácií v závislosti na hĺbke, ako aj profilmi s maximom, alebo aj sigmoidálneho tvaru. Štandardný modelový prístup, založený na Richardsovej rovnici a konvektívno-disperznej rovnici, predpovedal viac vyplaveného Cl^- ako bolo pozorované v poli. O niečo lepšie výsledky boli dosiahnuté, ak sa potenciálna transpirácia zvýšila 1,5-násobne. Lepšie výsledky v prognóze vyplavovania solí boli dosiahnuté, ak model obsahoval separátne mobilnú a imobilnú vodu, predpovšetkým zlepšením tvarov vertikálnych rozdelení koncentrácií chlóru. V tejto štúdii bolo ukázané, aké je dôležité presné určenie dolných okrajových podmienok, priestorovej variability rýchlosti infiltrácie, ako aj určenie výparu z povrchu pôdy a transpirácie.

KĽÚČOVÉ SLOVÁ: transport rozpustených látok, simulácia v poľných podmienkach, chloridy, Unsatchem.

1. Introduction

Soil salinization is a long-standing problem for irrigated agriculture in arid and semiarid regions (*Hillel*, 1998). In the San Joaquin Valley of California the problem of soil salinization is not as acute as in many other areas of the world, but still a major concern, especially in areas with relatively shallow water tables (< 3 m). Also, a positive correlation has been established between soil salinity, boron and selenium concentrations in this area (*Deverel* and *Millard*, 1988). Considering the soil salinization challenges and associated environmental problems due to elevated selenium concentrations at the Kesterson reservoir resulting from agricultural drainage (*Benson* et al., 1991), a need exists for accurate prediction of solute loadings from agricultural areas that are drained.

Regional studies of salinity on the west side of the San Joaquin Valley demonstrated that the most salt-affected soils are fine-grained deposits located on the margins of alluvial fans that are downslope from the Diablo Range (*Deverel* and *Gallanthine*, 1989). The spread of irrigated agriculture in this area changed the dynamics of discharge and recharge to groundwater from predominantly horizontal flow to vertical flow due to evapotranspiration and infiltration in cropped fields (*Deverel* and *Gallanthine*, 1989; *Belitz* and *Phillips*, 1995). Regional studies of groundwater and its salinization need accurate representations of water flow and salt loadings to groundwater from the overlying vadose zone.

Variably saturated water flow and solute transport in the vadose zone are commonly modeled using the Richards equation and the convection-dispersion equation, respectively (*Nielsen* et al., 1986; *van Genuchten* and *Simunek*, 2004). Other approaches include state-space models (*Wu* et al., 2001), mobile-immobile flow models (*van Genuchten* and *Wierenga*, 1976) and reformulations of solute transport models within a transfer function context (*Jury* and *Roth*, 1990). Much evidence exists that the standard CDE equations often do not accurately predict solute transport in undisturbed field soils (*Jarvis* and *Larsson*, 2001). For example, *Dust* et al. (2000) observed that near-surface bromide concentrations in a sandy soil exceeded predictions obtained with the LeachP model. *Mohanty* et al. (1998) similarly were unable to predict water and solute transport to tile drains using traditional flow and transport equations (*Simunek* et al., 1996a). Solute leaching in field soils under natural weather conditions also could not be modeled successfully using the CDE (*Snow* et al., 1994; *Jacques* et al., 2002). However, the CDE in several other cases adequately represented pesticide and solute transport under field conditions (*Wagenet* and *Hutson*, 1986; *Suarez*, 2001).

Considering all of these studies, it is clear that modeling of vadose-zone transport in field soils is subject to considerable uncertainty. Potential sources of uncertainty are the presence of preferential or non-equilibrium flow (*Nkedi-Kizza* et al., 1985; *Simunek* et al., 2003) and lack of detail in the specification of upper and lower boundary conditions, plant root water uptake, rooting distribution and spatial variability in the material properties. When preferential flow occurs, the flowing water bypasses certain parts of the soil profile, thereby resulting in more rapid transport of solutes in the preferential flow regions and slower transport in the soil matrix (*Simunek* et al., 2003). Assuming the presence of immobile water is one approach for treating preferential flow (*van Genuchten* and *Wierenga*, 1976).

Despite the above uncertainties numerous modeling studies are still useful in attempts to better understand and/or predict the movement of agricultural and other contaminants in the vadose zone. One example is the evaluation of remediation strategies for salt-affected soils (*Suarez*, 2001). Prediction of pesticide movement in soil is similarly important for development of management practices that will maximize the effectiveness of the pesticide usage, and minimize their potential for contamination of ground or surface waters (*Wagenet* and *Rao*, 1990).

The current study is part of a larger project designed to estimate salt loadings from irrigated areas in the San Joaquin Valley through the vadose zone to groundwater. As part of that project we conducted extensive soil sampling within a single agricultural field during a two-year period. The objective of the current study was to test alternative models of chloride transport in order to evaluate their predictive capability with respect to chloride concentrations in the 1.8-m thick vadose zone. Agricultural productivity on the west side of the San Joaquin Valley is affected by boron and, to a lesser

extent, selenium. Developing field-applicable modeling of chemical transport for Cl^- is hence a necessary first step for modeling transport of these elements that form reactive oxyanions.

This study differs from previous field studies in several ways. First, our intention was to apply a set of recommended procedures for utilizing the models when data sets are incomplete. For example, we utilized standard measurements of soil texture and bulk density to estimate soil hydraulic properties based on pedotransfer functions, rather than actual measurements. Also, we developed soil surface boundary conditions for water flow based on the California Irrigation Management Information System (CIMIS) estimates of the potential evapotranspiration rate, CIMIS crop coefficients, measured precipitation, and an assumed uniform distribution of irrigation water throughout the field. Second, we wanted to conduct simulations that ran continuously for a two-year period, thereby including simulations of both crop growth and fallow periods in the fall and winter. Finally, we wanted the study to apply to the entire field with all of its natural variability. For this purpose we conducted soil sampling and simulations at 45 different locations in the field.

2. Methods

2.1 Field experiment

The study was conducted in a 65 ha agricultural field located approximately 100 km west of Fresno in the Broadview Water District, San Joaquin Valley, California. Soils at the field site consisted of a Cerini series, fine-loamy, mixed (calcareous), superactive, thermic Fluventic Haplocambids, and a Tranquillity series, very fine, smectitic, thermic Sodic Haploxerert. The Cerini clay-loam occurred in a broad band trending SW-NE through the center of the field. The Tranquillity clay was present in 10% of the field area in the NW and SE corners (*Wu* et al., 2001).

Soil sampling locations were laid out on a 6 x 6 square grid with a spacing of 140.4 m. In addition to 36 grid sites, 9 more sites at other locations within the field were sampled (Fig. 1). These sites were identified in 1994 during a study of local groundwater levels. Soil sampling took place during the weeks starting November 13, 1995, April 15, 1996, July 15, 1996, May 12, 1997 and November 10, 1997. Six soil samples were collected from a single borehole at each location. The core sample tube in each case was 0.05 m in diameter, with samples taken at 0.3 m increments to a depth of 1.8 m. Observation wells were located on the 6 x 6 grid and installed during the growing seasons in 1996 and 1997. These wells provided depth-to-water measurements and groundwater samples for chemical analyses. The groundwater chemical compositions of the 9 extra sites were estimated from nearby wells using inverse-distance-squared weighting.

During the experimental study (1994 through 1997) the water table in the field was manipulated as part of a subsurface irrigation experiment. This was accomplished by controlling flow within the field's E-W tile-drain laterals. The seven tile-drain laterals were spaced 123 m apart and installed at a depth of 1.5–1.8 m. Valves installed at the eastern end of tile drain laterals were adjusted to control the groundwater level. When the valves were adjusted for higher water levels, water pressures increased in the tile drains and at times may have reversed the normal flow direction.

2.2 Soil chemical analysis

Soil samples were extracted at room temperature (~22 °C) with deionized water at a 1:1 ratio based on mass. Chloride analyses of the extract were performed using coulometric titration (*Cotlove* et al., 1958). The concentrations were recalculated to field water contents based on conservation of Cl^- mass.

2.3 Hydraulic Properties

Particle size analyses were performed on 40-g soil samples representing six depths at each of the 45 locations. Sand fractions were determined by sieving, silt and clay fractions using the hydrometer method. Bulk densities were determined for soil cores, 0.05 m in diameter and 0.3 m long. Prior to weighing, the soil was dried at 100°C until no further weight loss was detected. Water retention parameters, including the saturated water content (θ_s), the residual water content (θ_r), and the shape parameters α and n (*van Genuchten*, 1980), were estimated using the Rosetta computer program based on a hierarchical artificial neural network approach (*Schaap* et al., 1998). Estimates were obtained using the bulk density and texture as determined by particle size analyses (Fig. 2). The saturated hydraulic conductivity (K_s) was also estimated with Rosetta. An upper limit was established at 0.8 m d^{-1}

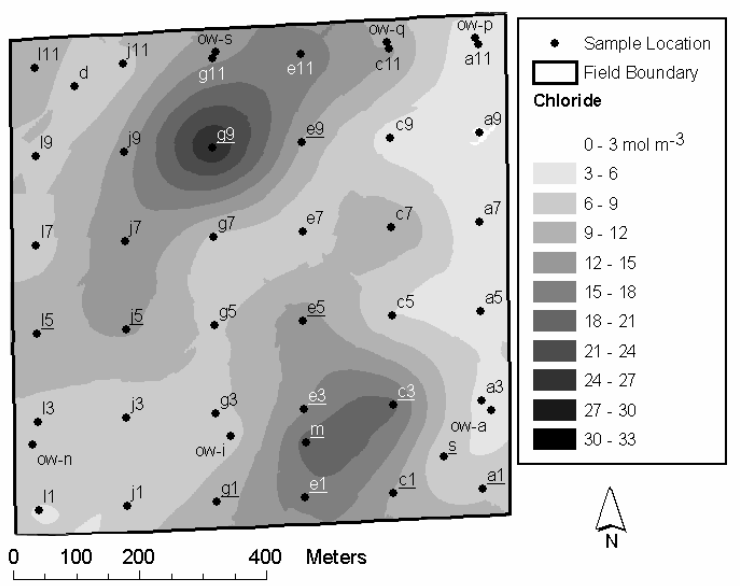

Fig. 1. Sampling locations and kriged surface of mean Cl^- concentration in the 0.0–1.8 m depth range (November, 1997). Underlined labels signify Cl^- maxima in the profile.
Obr. 1. Lokality odberu vzoriek pôdy a krigované povrchy priemernej koncentrácie Cl^- v hĺbkach 0,0–1,8 m (november 1997). Značky označujú maximá Cl^- v profile.

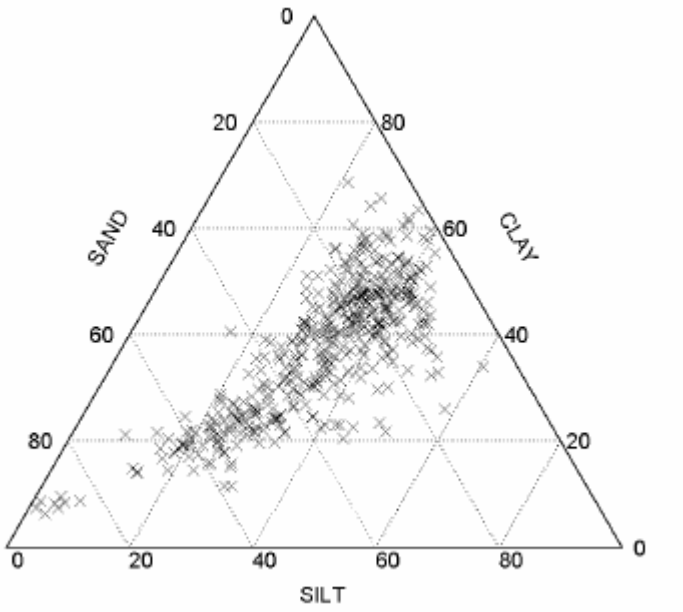

Fig. 2. Soil texture in three fractions for 45 locations and six depths.
Obr. 2. Textúra pôdy v 45 lokalitách a v šiestich hĺbkach.

in order to obtain stable behavior in the water flow calculations. This constraint was needed for only 2 of 258 estimated values at 43 locations where computations were successful, and hence was not significant. A potentially more significant source of error was the development of a possible capillary barrier at locations where the hydraulic conductivity was high due to the presence of sand lenses. A one-dimensional model is not suited to deal with possible lateral flow due to this layering. Hydraulic parameters (θ_s, θ_r, α, n, K_s) were specified for six soil layers of which the top five layers were 0.3 m thick, while the hydraulic properties of the 1.5–1.8 m layer were extended to the lower boundary of the finite-element model at 3 m depth.

2.4 Solute Transport Models

Water flow and multicomponent chemical transport were simulated for a two-year period starting in November 1995 at 45 locations in the field (Fig. 1). Other processes modeled in this simulation were CO_2 flux, heat flow, root water uptake and root growth. The CO_2 flux and heat flow, while not significant for chloride transport, were needed for a companion study of boron transport (*Vaughan* et al., 2004). Water flow was calculated using a finite-element numerical solution of the Richards equation. Solute transport was modeled using either the standard convection-dispersion equation (CDE) or the mobile-immobile water model (MIM). For the CDE simulations, multicomponent chemical transport was modeled using

$$\frac{\partial \theta_w c_k}{\partial t} + \rho\left[\frac{\partial \overline{c}_k}{\partial t} + \frac{\partial \hat{c}_k}{\partial t}\right] = \frac{\partial}{\partial z}\left[\theta_w D \frac{\partial c_k}{\partial z} - q c_k\right] \quad (1)$$

as incorporated in the Unsatchem code (*Simunek* et al., 1996b). In Eq. (1), θ_w is the volumetric water content [m^3 m^{-3}], c_k – the concentration of the kth species in the soil solution [mmol L^{-1}], $\overline{c}_k$ – the total surface concentration of the kth species [mmol kg^{-1}], $\hat{c}_k$ – the total concentration of the kth species in solid phases [mmol kg^{-1}], ρ – the bulk density of the soil [Mg m^{-3}], D – the dispersion coefficient [m^2 s^{-1}], and q – the water flux [m s^{-1}]. The dispersion coefficient was calculated using

$$\theta_w D = \lambda |q| + \theta_w D_m \tau_w, \quad (2)$$

where λ is the dispersivity [m], D_m – the molecular diffusion coefficient in free water [m^2 d^{-1}], and τ_w is a dimensionless tortuosity factor ($\tau_w = \theta_w^{7/3}/\theta_s^2$) (*Simunek* et al., 1996b). The dispersivity and molecular diffusion coefficient are given in Tab. 1.

For the MIM simulations the CDE was modified to consider two different types of soil water, a mobile fraction and an immobile fraction (*van Genuchten* and *Wierenga*, 1976).

$$\theta_w = \theta_m + \theta_{im}, \quad (3)$$

where θ_m is the mobile water content and θ_{im} – the immobile water content. In our implementation of the MIM model, the immobile water content during the transient simulations was defined as

$$\theta_{im} = \theta_r + \eta(\theta_w - \theta_r), \quad (4)$$

where η is a dimensionless parameter varying between zero and one. We assumed that the residual water (θ_r) was always immobile. The transport equation for the MIM model is

$$\begin{aligned} &\frac{\partial}{\partial t}\left[\theta_m c_{k,m} + \theta_{im} c_{k,im}\right] + \\ &\rho \frac{\partial}{\partial t}\left[\hat{c}_{k,m} + \overline{c}_{k,m} + \hat{c}_{k,im} + \overline{c}_{k,im}\right] = \\ &\frac{\partial}{\partial z}\left[\theta_w D \frac{\partial c_{k,m}}{\partial z} - q_m c_{k,m}\right], \end{aligned} \quad (5)$$

where the variables and constants have the same meaning as in Eq. (1) but apply to either mobile (subscript *m*) or immobile (subscript *im*) water.

For the purpose of calculating solute transport, the water flow velocities for the mobile water fraction were increased from values calculated with the Richards equation by a factor equal to θ_w/θ_m ($q_m = q_w\theta_w/\theta_m$). The MIM modification of the CDE involves the simultaneous solution of Eq. (5) for the mobile fraction and a mass transfer equation expressing the transfer rate of solutes between the two water fractions:

T a b l e 1. Miscellaneous model parameter values.
T a b u ľ k a 1. Parametre modelu.

Parameter	Value	Unit
1. Molecular diffusion coefficient in free water*	1.0×10^{-4}	[m^2 d^{-1}]
2. Longitudinal dispersivity**	0.05	[m]
3. Critical value for product of grid Peclet and Courant numbers***	2.0	[–]
4. CO_2 concentration at soil surface	3.6×10^{-4}	[PPMV]
5. CO_2 concentration at 3 m depth	0.02	[PPMV]
6. Diurnal, sinusoidal temperature amplitude at soil surface	5	[°C]
7. Maximum depth of water layer at soil surface	0.05	[m]

**Flury* et al., 1999; ***van Hoorn*, 1981; ****Simunek* et al., 1996b
1 – súčinitel molekulárnej difúzie v čistej vode, 2 – pozdĺžna disperzivita,3 – kritická hodnota súčinu Pécletovho a Courantovho čísla v uzle, 4 – koncentrácia CO_2 na povrchu pôdy, 5 – koncentrácia CO_2 v hĺbke 3 m, 6 – denná sinusoidálna amplitúda teploty na povrchu pôdy, 7 – maximálna hrúbka vrstvy vody na povrchu pôdy.

$$\frac{\partial \theta_{im} c_{k,im}}{\partial t} = \omega (c_{k,m} - c_{k,im}) . \quad (6)$$

The MIM model has two additional parameters, the immobile volumetric water content (θ_{im}) and the mass transfer coefficient (ω) representing material properties. Tab. 1 provides material property values and other data that were kept constant in the simulations.

Eqs (5) and (6) were solved numerically by means of a one-dimensional Galerkin finite-element approach similar to that described by *Simunek* et al. (1998). The vertical flow domain at each location was 3 m in length and was discretized into 377 elements. Nodal spacings varied exponentially from 3.0 x 10^{-3} m at the top to 0.03 m at a depth of 2.7 m. Nodal spacings below this depth decreased linearly in order to maintain stability in the transport calculations near the base of the simulated profile.

The mass balance error due to numerical approximations such as spatial and temporal discretizations can be calculated as the difference between a true value, the sum of the integrated Cl^- fluxes at the boundaries of the column and the initial mass, and the current Cl^- mass in the column. The maximum absolute value of the mass balance error for the CDE model was found to be negligible. For all MIM simulations the maximum error was 0.07 $mmol_c$ when the total mass in the column was 7.1 $mmol_c$, for a relative error of 1%.

2.5 Field Crops and Irrigation

The field was cropped to tomato (Lycopersicon lycopersicum L.) in 1996 and cotton (Gossypium hirsutum L.) in 1997. Root water uptake was simulated using

$$S(h, h_\varphi) = \alpha_s(h) \alpha_\varphi(h_\varphi) S_p , \quad (7)$$

where h_φ is the osmotic head [m], S_p – the potential root water uptake distribution [$m^3\ m^{-3}\ s^{-1}$] (*Simunek* et al., 1996b), $\alpha_s(h)$ – the water stress response function, and $\alpha_\varphi(h_\varphi)$ – the osmotic stress response function. The water stress response function was calculated using

$$\alpha_s(h) = [1 + (h / h_{50})^b]^{-1} , \quad (8)$$

where h_{50} and b are crop-specific parameters (*Simunek* et al., 1996b). For tomato h_{50} = -5 m, b = 2 and for cotton h_{50} =-25 m, b = 2. The values for cotton were estimated from results for alfalfa (*Homaee* et al., 2002). The value of h_{50} for tomato was estimated by assuming a relatively high potential evapotranspiration rate of 6.4 mm d^{-1} (*Hillel*, 1998; p. 568). For osmotic stress, a similar equation, with the pressure head replaced by the osmotic head (h_ϕ), has the parameters $h_{\varphi 50}$ = –100 m and b = 3 for tomato and $h_{\varphi 50}$ = –178 m and b = 3 for cotton (*van Genuchten* and *Gupta*, 1993). Rooting depth was calculated as the product of the Verhulst-Pearl logistic growth function and the maximum rooting depth (*Simunek* et al., 1996b). The maximum rooting depth for tomato was 1.2 m for tomato and 3.0 m for cotton. However, the program was modified to reset the maximum rooting depth for cotton to 0.1 m below the water table.

Tomato was irrigated using gated-pipe water delivery to furrows, while cotton was furrow-irrigated with siphon-tube delivery at the upper end of the furrow. Sprinklers were used for the pre-irrigations in February of each year, prior to planting. The precision of water delivery to the 65 ha field, as determined from the precision of the gauge (0.1 acre-feet), was approximately 0.2 mm depth. Distribution non-uniformity was probably a greater source of error in calculations of the infiltration rate.

2.6 Initial Conditions

Initial volumetric soil water contents were calculated from measurements of the gravimetric water content and bulk density (Fig. 3). The gravimetric water contents were determined by drying at 100°C until no further weight change occurred. Initial pressure heads were calculated from water retention functions utilizing hydraulic properties determined with the Rosetta program (*Schaap* et al., 1998). Initial resident Cl^- profiles were determined by analysis of soil samples taken in November 1995 (Fig. 3).

2.7 Boundary Conditions

The atmospheric boundary conditions for water flow at the soil surface alternatively involved time-dependent prescribed fluxes and, if ponding occurred, prescribed pressure heads (*Simunek* et al., 1996b). Precipitation data were combined with irrigation data to build a continuous record of the potential water flux at the soil surface for the two-year simulation period starting November 1, 1995. Calculations of the potential water flux assumed

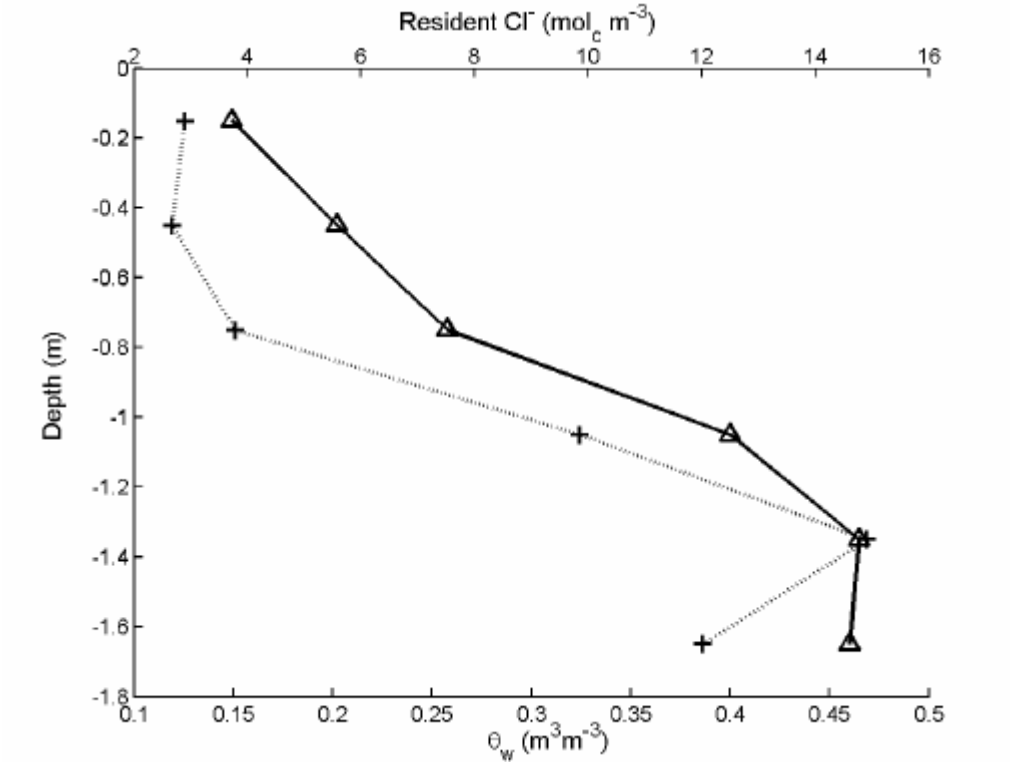

Fig. 3. Measured initial resident Cl^-(+) and volumetric water content (θ_w). Data shown are median values for 45 locations.
Obr. 3. Merané počiatočné rezidentné Cl^-(+) a objemový obsah vody (θ_w). Údaje sú mediánom pre 45 lokalít.

that irrigation water was applied uniformly over the field. While a necessary simplification for our one-dimensional simulations, this boundary condition likely was unrealistic for furrow-irrigation of both crops. Possible development of ponding or runoff was determined during the simulations. Irrigation in both years was carefully managed to ensure that water did not run off the field. A maximum water layer of up to 0.05 m was allowed to build up, thereby ensuring that no runoff was modeled. The total depth of water applied to tomato, including the pre-irrigation in February 1996, was 0.69 m. The same total amount for cotton in 1997 was 0.85 m.

Transfer of water from the soil to the atmosphere occurred by evaporation at the soil surface and by plant transpiration. Input data for calculating evaporation and transpiration rates were either daily potential soil evaporation and transpiration when the field was cropped, or daily potential soil evaporation at other times. Both types of data were computed from CIMIS weather station data recorded at the Panoche station some 20 km northwest of the field. The daily potential evapotranspiration rate was calculated as the product of a crop coefficient and the reference crop evapotranspiration rate reported each day by the station. Crop coefficients for the San Joaquin Valley were taken from CIMIS leaflet #21427[1)]. The CIMIS daily reference evapotranspiration was calculated from a modified Penman equation with a 0.10–0.15 m grass cover as the reference crop (*Doorenbos* and *Pruitt*, 1977). Potential soil evaporation rate was calculated from the reference crop evapotranspiration rate using an expression for calculating bare soil potential evaporation from reference crop evapotranspiration (*Snyder* et al., 2000). The potential transpiration rate was then estimated as the difference between the potential evapotranspiration rate and the potential soil evaporation rate.

The soil surface evaporation model requires specification of a minimum value of pressure head (h_{crit}) at the soil surface (*Simunek* et al., 1996b). In order to maintain numerical stability in the chemical speciation calculations we fixed h_{crit} at –25 m, which at first caused too high estimates of the soil

[1)]Available from DWR-DLA-WCO, 1020 9th Street, 3rd Floor, Sacramento, CA 95814.

evaporation rates. This problem was avoided by specifying the potential soil evaporation rate after a soil wetting event using a square-root-of-time expression (*Tanner* and *Jury*, 1976; *Black* et al., 1969). During and for 2 days after an irrigation event, potential soil evaporation rates were set equal to the bare soil potential evaporation rate (*Snyder* et al., 2000). After two days of drying, the potential evaporation rate was reduced using the square-root-of-time expression with an empirical constant $C = 0.4$ (*Black* et al., 1969). Keeping h_{crit} as –25 m during the first two days ensured that the actual soil evaporation rate matched the potential soil evaporation rate at all times during the simulations.

The lower boundary of the simulated profile was assumed to be 3 m below the soil surface, a depth that always remained below the fluctuating water table. Pressure heads at this boundary were determined from groundwater levels in wells situated on the same 6 x 6 grid as the sampling locations (Fig. 1). Weekly water table measurements were conducted during the growing season. At other times the water table was estimated from fitted bicubic surfaces using data from 18 permanent wells located within 3.3 km of the field. On three dates (July 1, 1996; July 9, 1997 and August 14, 1997) we had simultaneous readings of the in-field wells and the permanent wells. Mean water depths at well locations in the field estimated from measurements at the permanent wells were 1.50, 1.56 and 1.59 m greater than the measured in-field values for the three dates. Based on these results a correction of 1.55 m was applied to the water table estimates from the bicubic surfaces. For water flow a Dirichlet specified pressure head condition was applied to the lower boundary as determined from the water table measurements and estimates. For chemical transport the lower boundary concentration was a specified concentration as determined from chemical analyses of the groundwater at each location. These concentrations showed little change over the two-year period, thus allowing us to use a constant concentration boundary condition.

3. Results and Discussion

3.1 Field Data Analysis

Resident chloride concentrations ($mol_c\ m^{-3}$ soil) for the final sampling in November, 1997 were found to be highly variable among the 45 locations (for all measurements, CV = 142%). The arithmetic mean of chloride concentrations of the six samples taken from 0–1.8 m depth at each location varied between 2.5 and 30.2 $mol_c\ m^{-3}$. These mean values were kriged using ordinary point kriging with a spherical, isotropic semivariogram model. The areal distribution of the mean Cl^- concentration exhibited two maxima on either side of the northeast-southwest trending band of relatively low concentration (Fig. 1). The lowest Cl^- concentrations occurred along the eastern boundary of the field near the main drain connecting the seven tile drains that run east-west. The low Cl^- concentrations along the eastern boundary were likely influenced by some horizontal transport to the sump in the northeast corner.

3.1.1 Chloride Profile Shapes

Observed variations in the Cl^- concentration with depth may be classified by profile shape. Five different concentration distributions were identified: (1) monotonically increasing concentrations vs. depth, (2) monotonically decreasing concentrations, distributions having (3) minima, or (4) maxima, and (5) other shapes, including sigmoidal shapes. The "maximum" shape is used to describe locations where a maximum in the Cl^- concentration occurred at some point within the top 1.5 m of the profile. Figs 4 and 5 show examples of monotonically decreasing and maximum concentrations, respectively. The Cl^- profile shapes were predominantly monotonically increasing or of the maximum type (Tab. 2). Whereas the maximum shape was common for locations with high Cl^- concentrations, this shape was not found at any location where the mean Cl^- concentration for 0–1.8 m depth was less than 6 $mmol\ L^{-1}$. The spatial distribution of the maximum shapes was quite restricted. This shape occurred at all 9 locations in a triangular region near the southeast corner delineated by a1, e5 and g1 in Fig. 1, and additionally in a region northwest of the center of the field, including locations g9, e9 and j5.

The shapes of calculated Cl^- profiles were similarly classified as above. Since the shape classification is subject to some uncertainty the classification operation was repeated on three different days. The largest variation in the shape classification data of Tab. 2 was 10% for monotonically-increasing shapes that were obtained with the MIM simulations.

3.1.2 Correlation of Cl^- Concentration Among Different Sampling Periods

Depth-averaged resident chloride concentrations were calculated for each sampling except for the second sampling, in April, 1996, which was incomplete. Correlation coefficients were computed for these data to characterize temporal variations. The correlation coefficient matrix for the four complete

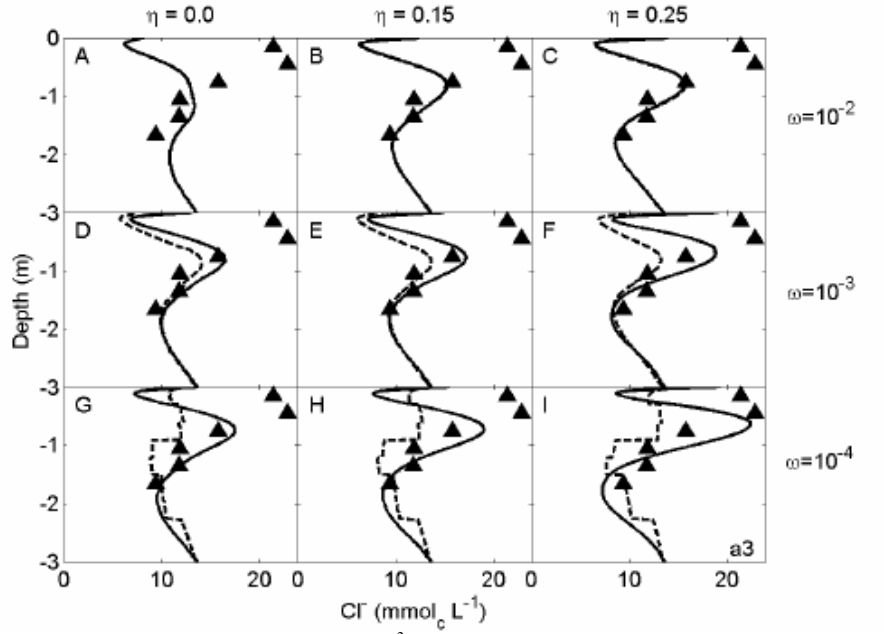

Fig. 4. Simulated in-situ Cl^- concentration profiles [$mol_c\ m^{-3}$] at location a3 for mobile (dotted) and immobile water (solid), and comparison with measured concentrations at six depths recalculated in terms of the in-situ water content. Plot A is for the CDE, and plots B through I are for the MIM using MIM parameter values as shown.

Obr. 4. Rozdelenia koncentrácií Cl^- [$mol_c\ m^{-3}$] v poľných podmienkach v lokalite a3 pre mobilnú (bodkované) a imobilnú vodu (plné), a porovnanie s meranými koncentráciami v šiestich hĺbkach, prepočítané na obsah vody in-situ. Tvar A je pre CDE a tvary B až I sú pre MIM, použijúc MIM hodnoty parametrov, ako je to uvedené.

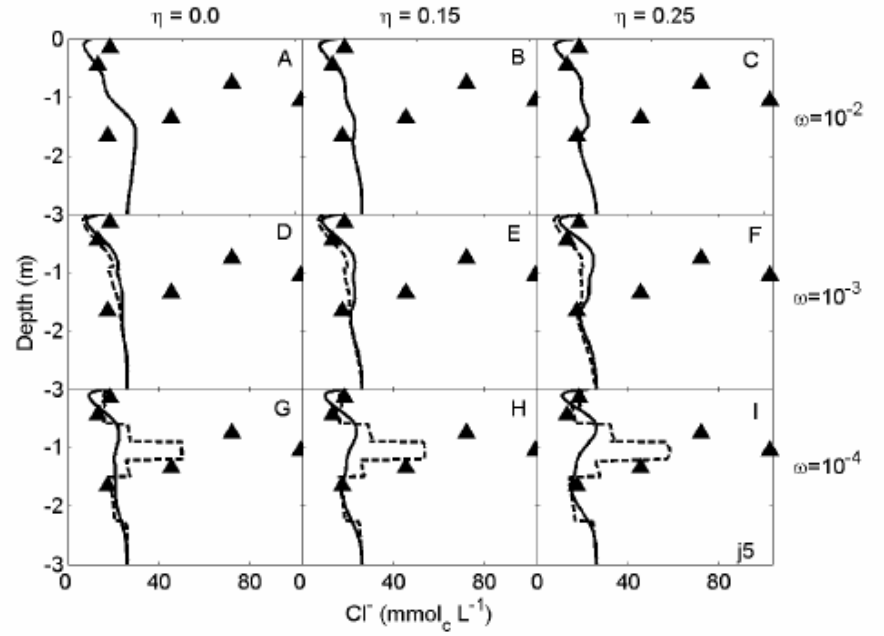

Fig. 5. Simulated in-situ Cl^- concentration profiles [$mol_c\ m^{-3}$] at location j5 for mobile (dotted) and immobile water (solid), and comparison with measured concentrations. Plot A is for the CDE, and plots B through I are for the MIM using MIM parameter values as shown.

Obr. 5. Rozdelenia koncentrácií Cl^- [$mol_c\ m^{-3}$] v poľných podmienkach v lokalite j5 pre mobilnú (bodkované) a imobilnú vodu (plné), a porovnanie s meranými koncentráciami. Tvar A je pre CDE, a tvary B až I sú pre MIM, použijúc MIM hodnoty parametrov, ako je to uvedené.

T a b l e 2. Cl^- profile shape comparison [%].
T a b u ľ k a 2. Porovnanie tvarov profilov Cl^-.

	Monotonically increasing[1)]	Monotonically decreasing[2)]	Minimum	Maximum	Other
Measured	49	4	7	31	9
CDE	91	0	0	0	9
MIM	44	0	0	41	15

1 – monotónne stúpajúce, 2 – monotónne klesajúce

samplings demonstrates that the time of year was an important factor determining the correlation (Tab. 3). The highest correlation coefficient (r) were found for the first and fifth samplings, both in November. The other values of r that exceeded 0.7 occurred for post-harvest samplings. Lower values of r were generated when samples taken in the spring were compared with post-harvest samples. This suggests that annual cyclic processes influenced Cl^- concentrations in the vadose zone.

3.2 Simulations

3.2.1 CDE Modeling

Simulations were conducted for a two-year period starting on November 1, 1995.

Measured Cl^- concentrations were determined for 0.3 m cores and, in order to compare the measured value with model results, it was necessary to calculate mean modeled concentrations for depth intervals corresponding to those that were sampled. Model results were compared with measured data from soil samples taken during four sampling periods starting in April 1996.

Initial simulations were conducted with potential transpiration rates fixed as values estimated from the Panoche CIMIS station evapotranspiration data. Considerable uncertainty exists in the CIMIS estimates of the reference crop evapotranspiration estimates since the CIMIS measurements were made approximately 20 km to the northwest. Calculated resident Cl^- concentrations for November, 1997, using the CDE model with CIMIS potential transpiration rates, were smaller than measured concentrations at all depths and all locations. Furthermore, no maxima were present in the Cl^- distributions with depth. This implied that upward transport of Cl^- near the soil surface was underpredicted. As a test of the effect of varying potential transpiration rates, simulations were carried out using potential transpiration rates that were 1.5 and 2.0 times higher, but without changing the potential soil surface evaporation rates.

Increasing the potential transpiration rate should lead to less leaching because of more upward transport. However, an initial set of CDE results using potential transpiration rates multiplied by a factor of 1.5 still produced overpredictions of Cl^- leaching for 38 out of 43 locations in November, 1997. The five locations where observed leaching was greater than predicted were all near the eastern boundary of the field (a7, a9, a11, ow-a, s). Simulations with doubled potential transpiration did not exhibit significant improvement over those with a factor of 1.5. Hence, subsequent simulations discussed here were performed with the potential transpiration increased by 1.5.

We used the scaled root mean square error (SRMSE) to represent discrepancies between model predictions and measured Cl^- concentrations,

$$SRMSE = \frac{100}{\overline{O}} \sqrt{\frac{\sum (P_i - O_i)^2}{N}} , \qquad (9)$$

where P_i are model predictions, O_i – observations and $\bar{o}$ is the arithmetic mean of N observations (*Vanclooster* et al., 2000). The median SRMSE for the standard potential transpiration rate for 43 locations was 82%, while for otherwise identical conditions the mean SRMSE was 76% when the potential transpiration rate was increased by a factor of 1.5. The predictive capability of the CDE varied substantially depending on location. One of the better predictions for all four sampling times was for location ow-s (Fig. 6). Nonetheless, even at this location, calculated resident Cl^- concentrations in November 1997 were significantly less than the measured values at the four lowest sampling depths.

The measured chloride concentrations exhibited approximately lognormal distributions areally across the field at each of the six depths. A z-test was conducted to determine the significance of differences in the means of $\log_{10}(Cl^-)$ for the final concentrations predicted with the model, and the measured values from the November 1997 sampling. At $\alpha = 0.01$ the test statistic exceeded the critical value of 2.58, thus indicating a significant

T a b l e 3. Depth-averaged Cl^- correlation coefficients.
T a b u ľ k a 3. Súčinitele korelácie Cl^- spriemerované po hĺbke; 1 – dátum odberu vzoriek pôdy.

Sampling date[1)]	Sampling date	*r*
November, 1995	July, 1996	0.73***
November, 1995	May, 1997	0.40**
November, 1995	November, 1997	0.87***
July, 1996	May, 1997	0.45**
July, 1996	November, 1997	0.78***
May, 1997	November, 1997	0.41**

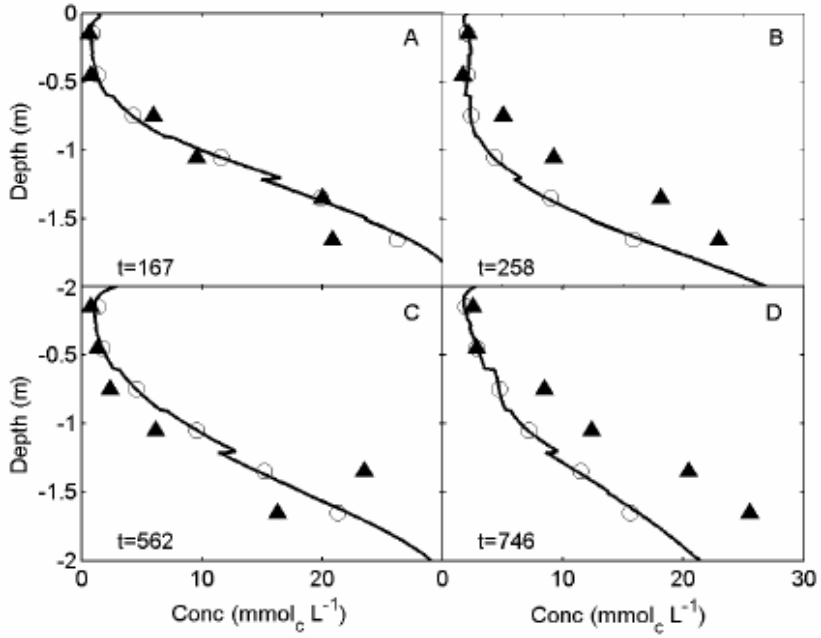

Fig. 6. Profiles of the resident Cl^- concentration [mol_c m^{-3}] at location ow-s obtained with the CDE at four sampling times (as indicated in the lower left of the plots, where *t* is the number of days starting November 1, 1995). Circles are simulated concentrations averaged over 0.3 m depth intervals. Measured data are shown by triangles.
Obr. 6. Rozdelenia koncentrácií Cl^- [mol_c m^{-3}] v poľných podmienkach v lokalite ow-s vypočítané s CDE pre štyri termíny odberov vzoriek pôdy (ako je to ukázané vľavo dolu na políčku, kde *t* je počet dní, počínajúc od 1. novembra 1995). Krúžkami sú označené simulované koncentrácie spriemerované pre intervaly hĺbok 0,3 m. Merané hodnoty sú označené trojuholníkmi.

difference in the means for samplings in the 0–1.5 m range. For the lowest depth range, 1.5–1.8 m, the test produced $z = 2.19$, which indicates that the null hypothesis that the two means represented the same population could not be rejected at $\alpha = 0.01$. At this point the mobile-immobile model (MIM) features were incorporated in the model to determine whether the separation of Cl^- between the mobile and immobile water fractions would lead to better simulations of the Cl^- field data.

3.2.2 Mobile-immobile water modeling

Model parameters required for the MIM model are the mass transfer coefficient (ω) and the immobile water content parameter (η). The tracer methods for obtaining MIM parameter values using tension infiltrometers (*Clothier* et al., 1992; *Jaynes* et al., 1995; *Al-Jabri*, 2002) could, at least in theory, be applied to this field. However, given the large spatial variations in texture, this would have required an inordinate number of measurements, well beyond the scope of our field measurement program. Instead, we elected to perform exploratory simulations in which the MIM parameters were varied systematically within certain ranges, i.e., $10^{-4} \leq \omega \leq 10^{-2}$ d^{-1}, and $0.0 \leq \eta \leq 0.25$. Optimal values of the two parameters for these ranges were determined by locating the minimum in the SRMSE (Eq. (8)). We found that simulations could not be reliably performed for η values above 0.25 without inducing numerical instabilities due to high effective velocities of the mobile water. This problem was more acute at locations having a highly variable saturated hydraulic conductivity of the different layers.

Calculated in-situ Cl^- concentrations were plotted for various (η, ω) pairs and compared with measured in-situ Cl^- concentrations sampled in November, 1997 at location a3 (Fig. 4). The solid line in subplot A is the Cl^- profile for a single CDE simulation. For the remaining MIM subplots, η had values of 0.0, 0.15 and 0.25 that increased horizontally across Fig. 4, while ω varied within the range $10^{-4} \leq \omega \leq 10^{-2}$. Higher values of η yielded higher effective water flow velocities in both directions and caused increasingly larger variations in Cl^- for all values of ω (Fig. 4). Concentration distributions versus depth of Cl^- in the mobile fraction were generally smooth, and diverged from Cl^- in the immobile fraction as ω decreased. As to be expected, the curves for the mobile and immobile Cl^- concentration were almost identical when ω was relatively large ($\omega = 10^{-2}$), thus reflecting rapid exchange between the two liquid regions. Plots G,H and I showed the smallest ω values ($= 10^{-4}$) and exhibited the largest separation in Cl^- profiles between the mobile and immobile regions.

At location j5, neither model was able to reproduce the peak concentration observed in November 1997. In particular, this was the case for all MIM simulations performed with varying values of η and ω (Fig. 5). Application of the MIM to location ow-s produced better agreement between the measured resident Cl^- concentration and the model results for ($\eta = 0.25$, $\omega = 10^{-4}$) as compared to other parameter values and the CDE results (Fig. 7).

The MIM simulations produced a higher percentage of Cl^- concentrations greater than measured in the 0–0.3 m depth range (45% compared to 16% for CDE). For the MIM the median SRMSE for this depth range was 22% compared to 41% for the CDE, thus indicating that the MIM model performed substantially better than the CDE in the uppermost 0.3 m.

The SRMSE for each location was calculated for varying values of the two MIM parameters. Contouring this statistic was a convenient way of studying the combined, interactive effects of the two parameters on the calculations, including comparisons with the data (Fig. 8). Based on plots of this type we obtained optimal values of the MIM parameters for each location. For 33 of the 36 locations on the 6 x 6 grid, the best agreement between model results and data were obtained for the following combinations: 52% for ($\omega = 10^{-4}$; $\eta = 0.25$), 3% for ($\omega = 3.2 \times 10^{-3}$; $\eta = 0.25$), 9% for ($\omega = 10^{-4}$; $\eta = 0.0$), and 36% for ($3.2 \times 10^{-3} \leq \omega \leq 10^{-2}$; $\eta = 0.0$). These results indicate that the MIM provided better agreement for low values of the transfer coefficient and/or high values of η at 64% of the 33 locations on the grid. For the remaining locations (36%), no significant improvement over the CDE was apparent. The distribution of η was found to be bimodal with 55% of locations having the minimum SRMSE when $\eta = 0.25$ and the remaining 45% when $\eta = 0$. No significant correlation was found between the optimal MIM parameter values and soil texture or bulk density. Three of the 36 locations were not considered in the MIM analysis above since high immobile water contents, in association with rapid flow, caused numerical inaccuracies in the solute transport computations.

3.2.3 Cl^- Profile Shape Classification

The mean weighted Cl^- concentration of the combined irrigation and precipitation fluxes during the simulation period was 1.9 $mmol_c\ L^{-1}$, and the mean lower boundary Cl^- concentration for all locations, 17.7 $mmol_c\ L^{-1}$. This implies that solutions of the transport equation, generally, should show an increase in Cl^- concentration with depth. Computed Cl^- profiles were mostly consistent with this as 91% of the profiles for the CDE simulation were monotonically increasing (Tab. 2). However, only 49% of the measured Cl^- profiles were of this type. None of the CDE profiles showed a maximum although 31% of the measured profiles had this shape. The shapes of Cl^- profiles calculated using the MIM compared much better with the measured shapes (Tab. 2). In particular, 41% of the MIM simulations generated maxima, albeit with lower peak concentrations than those in the measured profiles. The MIM predictions qualitatively were also much closer to the field data, although still with lower maximum concentrations as exemplified by the results in Fig. 5 for location j5.

3.2.4 Spatial Variations

Using the optimal MIM parameters for each location, the mean final Cl^- concentration over the 1.8 m deep vadose zone was calculated. The results were kriged using ordinary point kriging with a spherical, isotropic semivariogram model. Cl^- distributions were similar to those for the measured values (Fig. 9). Both maps had two maxima in approximately the same area of the field, and minima along both the eastern boundary and southwest

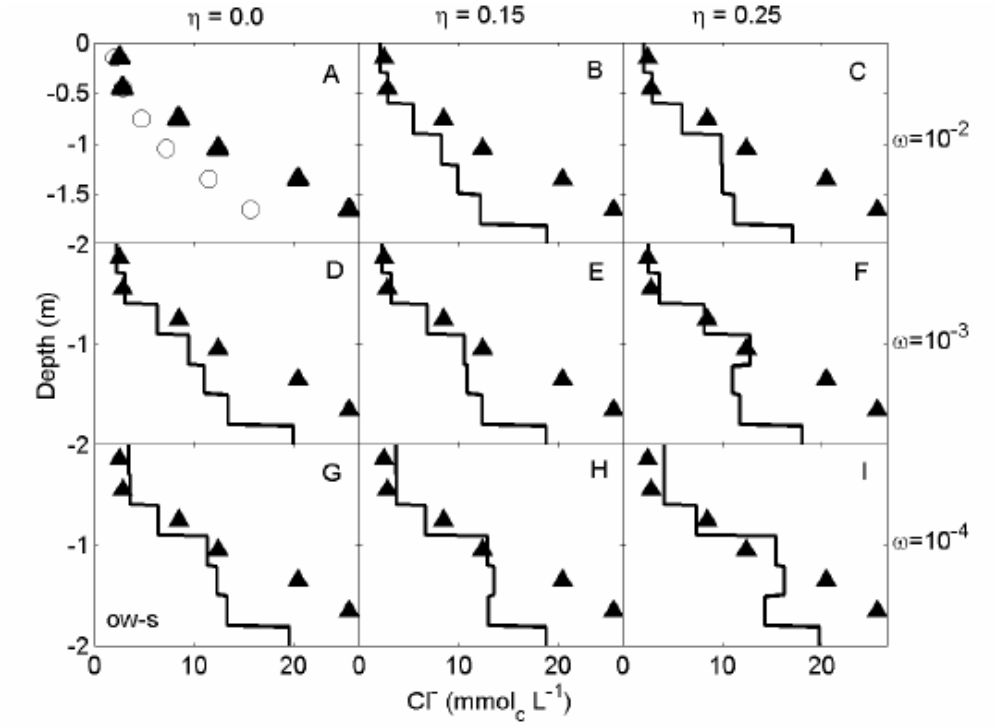

Fig. 7. Profiles of the resident Cl^- concentration [$mol_c\ m^{-3}$], including Cl^- in both water fractions, at location ow-s for November 1997. Plot A is for the CDE, and plots B through I for the MIM using MIM parameter values as shown.
Obr. 7. Rozdelenia koncentrácií Cl^- [$mol_c\ m^{-3}$] v lokalite ow-s pre obe frakcie vody v novembri 1997. Tvar A je pre CDE, a tvary B až I sú pre MIM, použijúc MIM hodnoty parametrov, ako je to uvedené.

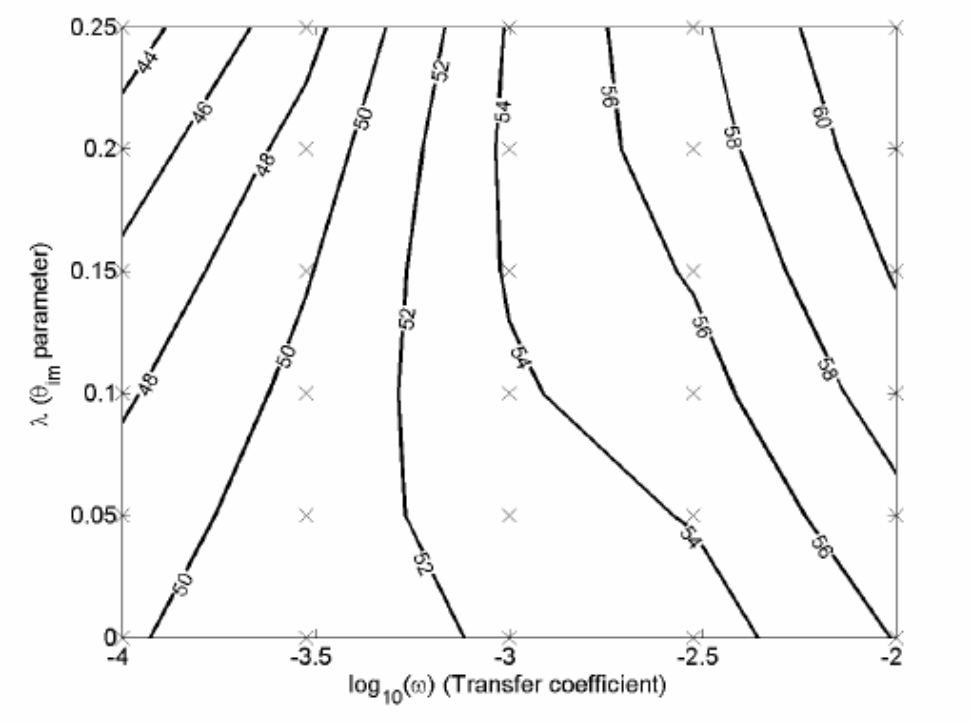

Fig. 8. Contouring of SRMSE at location ow-s based on simulations for 30 (η,ω) pairs represented by × symbols. The smallest SRMSE occurred for the pair (0.25, 10^{-4}).
Obr. 8. Obrysy SRMSE v lokalite ow-s zo simulácií pre 30 (η,ω) párov, reprezentovaných symbolmi ×. Najmenšie SRMSE boli získané pre dvojicu (0.25, 10^{-4}).

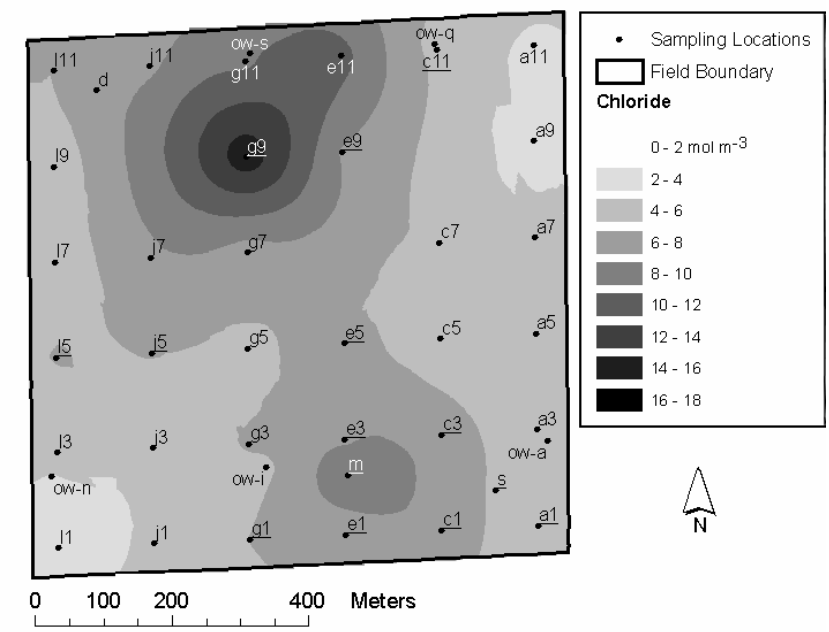

Fig. 9. MIM model results: kriged surface of the mean Cl^- concentration of the 0.0–1.8 m depth interval (November, 1997). Underlined labels signify Cl^- maxima in the profile.
Obr. 9. Výsledky modelu MIM: krigovaný povrch priemerných koncentrácií Cl^- v intervale hĺbok 0.0–1.8 m (november 1997). Podčiarknuté značky označujú maximá Cl^- v profile.

corner. The most noticeable difference was the lack of a distinct SW-NE trending minimum in the simulated data. Instead, a saddle with no distinct trend occurred near locations e5 and g5. The continuing, high Cl^- concentrations at g9, m and surrounding locations could not be simulated using either the CDE or MIM.

Considering that neither the CDE nor the MIM model was capable of reproducing the complexity of the observed Cl^- profiles, it is of interest to study the spatial distributions of the residuals. For all four sampling events subsequent to the initial sampling, the CDE model performed slightly better (SRMSE = 46.6%) than the optimal MIM model (SRMSE = 49.6%) for the six locations along the eastern boundary of the field. The median SRMSE for CDE at all other locations was 78.4% compared to 75.9% for the MIM. The Cl^- profiles with maxima tended to be geographically associated with high mean Cl^- concentrations in the profile. Both the CDE and MIM significantly underestimated the field data at these locations (Figs. 5 and 9). This suggests that improvements may be needed in the representation of the flow and transport processes at the field site, or the boundary conditions involved, in future efforts addressing the development of Cl^- concentration maxima.

3.3 Factors Potentially Affecting the Predictive Capability of Both Models

Water tables in the field during the experiment were managed as explained in the Methods section, i.e., groundwater levels were controlled by valves installed at the eastern ends of tile drain laterals while the field was cropped. Some uncertainty existed about the implications of this water table management on the lower boundary conditions. We believe that the overall effect was a reduction in leaching. Using a Dirichlet lower boundary condition for both the pressure head and the Cl^- concentration may have been more appropriate for locations near the eastern boundary of the field. These locations intersected a coarse-textured layer at about 1 m depth and could have drained easily toward the sump in the northeastern corner of the field, even with valves on the tile-drain laterals stopping normal flow. This may explain the lower SRMSE for these locations and the better performance here of the CDE model.

The accuracy of the mass balance of the modeled profiles and the discrepancies between the model predictions and the measured Cl^- concentrations imply that the simulated net downward fluxes of chloride through the lower boundary were greater than the measured Cl^- concentrations in November

1997 would indicate. The shapes of the Cl^- profiles were consistent with this conclusion. We found that 35% of observed profiles were either monotonically decreasing or showed maxima. These shapes must have been generated and maintained by greater upward movement of Cl^- than was predicted, particularly with the CDE model.

Mass balance discrepancies may have been caused by at least three factors: (1) neither model adequately represented the physical processes at the field site, (2) either the lower or upper boundary condition for water flow may have been poorly represented for at least some portion of the 2-year period, and (3) the root water uptake term in the Richards equation was incorrectly calculated for some depth range and time period during the simulations. Model inadequacy relates to the inability to represent certain processes that are known to occur. For example, a one-dimensional model cannot represent the effects of a sloping capillary barrier that may add horizontal components to the flow velocity. While generally it may be easy to list the various processes that potentially may have been poorly represented in a particular model, it is far more difficult to assess the relative importance of those processes to overall field-scale transport.

Our study suggests that the lack of specific data concerning water table fluctuations and groundwater composition during the field experiment may have contributed to a relatively poor definition of the lower boundary condition. The upper boundary condition was also subject to some uncertainty since potential evapotranspiration rates were determined for a CIMIS site located 20 km away from our field. Another possible source of uncertainty is the representation of the potential soil surface evaporation rate by a square root of time expression (*Black* et al., 1969). This simplification could be especially significant in the off-season when bare soil potential evaporation (*Snyder*, 2000) accounted for most or all of the upward water flux at and near the soil surface. For example, tillage events during the off-season could have caused substantially higher evaporative fluxes for the same reasons that these events cause increased CO_2 fluxes from soil to atmosphere (*Reicosky*, 1997). Finally, irrigation events were modeled by means of a uniform layer of water over the entire field. Some lateral nonuniform infiltration likely occurred due to local variations in the hydraulic conductivity. Also, nonuniform infiltration may have occurred along the furrows due to variations in opportunity times not accounted for by the model.

The sink term in the Richards equation accounting for root water uptake at a specified depth was determined using Eq. (7) involving the potential transpiration rate, the root water uptake distribution in the profile, and rooting depth. The potential transpiration rate had the same uncertainties with respect to applicability of the CIMIS data as the potential soil evaporation rate. While errors in the root water uptake distribution and rooting depth may have been important in calculations of the Cl^- profile shapes, they probably did not contribute significantly to the overprediction of leaching.

Future studies at this site should include local measurements of the latent heat flux to provide better constraints on the calculated evapotranspiration rates. Also, measurements of water table elevations throughout the year could provide data to evaluate whether more detailed representations of the lower boundary condition for water flow are necessary. The same is true for the solute transport boundary conditions near the water table.

4. Conclusions

Salinization of soils and salt loadings to groundwater are significant potential problems for agricultural productivity on the west side of the San Joaquin Valley. We attempted to model Cl^- transport in the upper 3 m of the soil profile at 45 locations in a 65-ha field in the San Joaquin Valley using both the standard CDE and alternative MIM options in the Unsatchem program. Soil sampling was done at these locations at five different times starting in November, 1995 and ending in November, 1997. The predictive capabilities of the models were evaluated by calculating the SRMSE for the four latter sampling events. The CDE model predicted substantially greater leaching than actually occurred. We addressed this problem by upgrading the model to account for MIM solute transport, and by increasing the potential transpiration rate by a factor of 1.5. Increasing the potential transpiration rate caused more upward chloride transport, thereby reducing the median SRMSE for the CDE from 82% to 76%. The MIM model simulations were conducted by systematically varying the two MIM model parameters (i.e., the immobile water fraction, η, and the mass transfer coefficient, ω). A set of simulations utilizing optimal values of these parameters improved predicted Cl^- profiles by reducing the median SRMSE to 72%. For 64% of the locations, mass transfer coefficients within the

range $10^{-4} \leq \omega \leq 10^{-3}$ together with relatively large immobile water contents, provided the best predictions.

The CDE and MIM models were further evaluated by comparing the shapes of predicted and measured Cl^- profiles. We found that the CDE model had a strong tendency to predict monotonically increasing resident Cl^- profiles vs. depth for November 1997. At the same time, measured chloride profiles exhibited a variety of shapes, including 31% having a maximum in Cl^- within the top 1.5 m. The MIM predicted maxima at 41% of the locations. Thus, predictions of profile shapes with the MIM model were substantially better than such shape predictions using the CDE. However, a significant deficiency of the MIM model was its inability to generate the large amplitude Cl^- maxima that were observed at some locations.

Future model studies may need to address the issue of how Cl^- maxima are generated and maintained in irrigated soil profiles including the origin of the areal distributions of the Cl^- maxima. This study also showed the importance of having accurate estimates of the evapotranspiration rate. For example, continuous measurement of the evapotranspiration rate in a field experiment using an eddy covariance system could provide a much-needed constraint. Further studies of the lower boundary condition of tile-drained fields with a water table transient are also warranted.

Ackowledgements. We acknowledge work done by Richard Schoeneman and Richard Soppe of the USDA Water Management Research Laboratory in Fresno. We are grateful to David Cone of the Broadview Water District for providing records of irrigation, precipitation and well depths. Salinity Laboratory staff who assisted in this study were JoAn Fargerlund and Jack Jobes.

REFERENCES

AL-JABRI S.A., HORTON R., JAYNES D.B., GAUR A., 2002: Field determination of soil hydraulic and chemical transport properties. Soil Sci., *167*, 353–367.

BELITZ K., PHILLIPS S.P., 1995: Alternative to agricultural drains in California's San Joaquin Valley: Results of a regional-scale hydrogeologic approach. Water Resour. Res., *31*, 1845–1862.

BENSON S.M., WHITE, A.F., HALFMAN S., FLEXSER, S., ALAVI M., 1991: Groundwater contamination at the Kesterson Reservoir. California 1. Hydrogeologic setting and conservative solute transport. Water Resour. Res., *27*, 1071–1084.

BLACK T.A., GARDNER W.R., THURTELL G.W., 1969: The prediction of evaporation, drainage, and soil water storage for a bare soil. Soil Sci. Soc. Am. Proc., *33*, 655–660.

CLOTHIER B.E., KIRKHAM M.B., MCLEAN J.E., 1992: In situ measurement of the effective transport volume for solute moving through soil. Soil Sci. Soc. Am. J., *56*, 733––736.

COTLOVE E., TRANTHAM H.V., BOWMAN R.L., 1958: An instrument and method for automatic, rapid, accurate, and sensitive tritration of chloride in biologic samples. J. Lab. Clin. Med., *51*, 461–468.

DEVEREL S.J., GALLANTHINE S.K., 1989: Relation of salinity and selenium in shallow groundwater to hydrologic and geochemical processes, western San Joaquin Valley, California. J. Hydrol., *109*, 125–149.

DEVEREL S.J. MILLARD S.P., 1988: Distribution and mobility of selenium and other trace elements in shallow groundwater of the western San Joaquin Valley, California. Environ. Sci. Technol., *22*, 697–702.

DOORENBOS J., PRUITT W.O., 1977:Guidelines for predicting crop water requirements. Irrigation and Drainage Paper 24, 2nd Ed. Food and Agriculture Organization of the United Nations, Rome, 156 p.

DUST M., BARAN N., ERRERA G., HUTSON J.L., MOUVET C., SCHAFER H., VEREECKEN H. and WALKER A., 2000: Simulation of water and solute transport in field soils with the LEACHP model. Agric. Water Manage, *44*, 1-3, 225–245.

FLURY M., YATES M.V. and JURY W.A., 1999: Numerical analysis of the effect of the lower boundary condition on solute transport in lysimeters. Soil Sci. Soc. Am. J., *63*, 1493–1499.

HILLEL D., 1998: Environmental Soil Physics. Academic Press, San Diego, CA.

HOMAEE M., FEDDES R A. and DIRKSEN C., 2002: Simulation of root water uptake II. Non-uniform transient water stress using different reduction functions. Agric. Water Manage., *57*, 111–126.

JACQUES D., SIMUNEK J., TIMMERMAN A. and FEYEN J., 2002: Calibration of Richards' and convection-dispersion equations to field-scale water flow and solute transport under rainfall conditions. J. Hydrol., *259*, 15–31.

JARVIS N., LARSSON M., 2001: Modeling macropore flow in soils: Field validation and use for management purposes. In: Conceptual Models of Flow and Transport in the Fractured Vadose Zone. pp. 189–215. National Academy Press. Washington D.C.

JAYNES D.B., LOGSDON S.D., HORTON R., 1995: Field method for measuring mobile/immobile water content and solute transfer rate. Soil Sci. Soc. Am. J., *59*, 352–356.

JURY W.A. and ROTH K., 1990: Transfer Functions and Solute Movement through Soil: Theory and Applications. Birkhauser-Verlag. Basel, 226 pp.

MOHANTY B.P., BOWMAN R.S., HENDRICKX J.M.H., SIMUNEK J. and VAN GENUCHTEN M. T., 1998: Preferential transport of nitrate to a tile drain in an intermittent-flood-irrigated field: Model development and experimental evaluation. Water Resour. Res., *34*, 1061–1076.

NIELSEN D.R., VAN GENUCHTEN M. T., and BIGGAR J.W., 1986: Water flow and transport processes in the unsaturated zone. Water Resour. Res., *22*, 89S–108S.

NKEDI-KIZZA P., BIGGAR J.W., SELIM H.M., VAN GENUCHTEN M.T., WIERENGA P.J., DAVIDSON J.M. and NIELSEN D.R., 1984: On the equivalence of two con-

ceptual models for describing ion exchange during transport through an aggregated Oxisol. Soil Sci. Soc. Am. J., *46*, 471–476.

REICOSKY D.C., 1997: Tillage-induced CO_2 emission from soil. Nutrient Cycling in Agroecosystems. *49*, 273–285.

SCHAAP M.G., LEIJ F.J. and VAN GENUCHTEN M.T., 1998: Neural network analysis for hierarchical prediction of soil water retention and saturated hydraulic conductivity. Soil Sci. Soc. Am. J., *62*, 847–855.

SIMUNEK J., HUANG K., SEJNA M. and VAN GENUCHTEN M.T., 1998: The HYDRUS-1D software package for simulating the one-dimensional movement of water, heat, and multiple solutes in variably-saturated media. Version 1.0, IGWMC-TPS-70, International Ground Water Modeling Center, Colorado School of Mines, Golden, Colorado, 186 pp.

SIMUNEK J., JARVIS N.J., VAN GENUCHTEN M.T. and CARDENAS A., 2003: Review and comparison of models for describing non-equilibrium and preferential flow and transport in the vadose zone. J. Hydrol., *272*, 14–35.

SIMUNEK J., SEJNA M. and VAN GENUCHTEN M.T., 1996a: The HYDRUS-2D software package for simulating water flow and solute transport in two-dimensional variably saturated media. Version 1.0, IGWMC-TPS-53, International Ground Water Modeling Center, Colorado School of Mines, Golden, CO, 167 p.

SIMUNEK J., SUAREZ D.L. and SEJNA M., 1996b: The Unsatchem software package for simulating one-dimensional variably-saturated water flow, heat transport, carbon dioxide production and transport, and multicomponent solute transport with major ion equilibrium and kinetic chemistry, Version 2.0. Research Report No. 141. US Salinity Laboratory, Riverside, California. 186 p.

SNOW V.O., CLOTHIER B.E., SCOTTER D.R. and WHITE R.E., 1994: Solute transport in a layered field soil – experiments and modeling using the convection-dispersion approach. J. Contaminant Hydrol., *16*, 4, 339–358.

SNYDER R.L., BALI K., VENTURA F. and GOMEZ-MACPHERSON H., 2000: Estimating evaporation from bare or nearly bare soil. J. Irrig. and Drain. Engng., *126*, 399–403.

SUAREZ D.L., 2001: Sodic soil reclamation: Modelling and field study. Aust. J. Soil Res., *39*, 6, 1225–1246.

TANNER C.B. and JURY W.A., 1976: Estimating evaporation and transpiration from a row crop during incomplete cover. Agron. J., *68*, 239–243.

VAN GENUCHTEN M. Th., 1980: A closed-form equation for predicting the hydraulic conductivity of unsaturated soils. Soil Sci. Soc. Am. J., *44*, 5, 892–898.

VAN GENUCHTEN M. Th. and GUPTA S.K., 1993: A reassessment of the crop tolerance response function. J. Indian Soc. Soil Sci., *41*, 730–737.

VAN GENUCHTEN M. Th. and SIMUNEK J., 2004: Integrated modeling of vadose-zone flow and transport processes. In: R.A. Feddes, G. H. de Rooij and J. C. van Dam (eds.), Unsaturated-Zone Modeling; Progress, Challenges and Applications, Wageningen UR Frontis Series, Vol. *6*, Chapter 2, pp. 37–69, x-xi, Kluwer Academic Publishers, Dordrecht, The Netherlands.

VAN GENUCHTEN M. Th. and WIERENGA P.J., 1976: Mass transfer studies in sorbing porous media 1. Analytical solutions. Soil Sci. Soc. Am. J., *40*, 473–480.

VAUGHAN P.J., SHOUSE P.J., GOLDBERG S., SUAREZ D.J. and AYARS J.E.., 2004: Boron transport within an agricultural field: Uniform flow versus mobile-immobile water model simulations. Soil Sci., *169*, 6, 401–412.

VAN HOORN J.W., 1981: Salt movement in unsaturated soil profiles. In: A. Verruijt and F.B.J.Barends (eds.). Flow and Transport in Porous Media. Rotterdam, the Netherlands: Balkema, 1981, 227–232 Proc. Euromech., 143. 2–4 Sept. 1981. Delft.

VANCLOOSTER M., BOESTEN J.J.T.I., TREVISAN M., BROWN C.D., CAPRI E., EKLO O.M., GOTTESBUREN B., GOUY V. and VAN DER LINDEN A.M.A., 2000: A European test of pesticide-leaching models: methodology and major recommendations. Agric. Water Mgmt., *44*, 1–19.

WAGENET R.J. and HUTSON J.L., 1986: Predicting the fate and of nonvolatile pesticides in the unsaturated zone. J. Environ. Qual., *15*, 315–322.

WAGENET R.J. and RAO B.K.,1983: Description of nitrogen movement in the presence of spatially variable soil hydraulic properties. Agric. Water Mgmt., 6, 227–242.

WU L., SKAGGS T.H., SHOUSE P.J. and AYARS J.E., 2001: State space analysis of soil water and salinity regimes in a loam soil underlain by shallow groundwater. Soil Sci. Soc. Am. J., *65*, 1065–1074.

Received 19. August 2004
Scientific paper accepted 8. February 2005

ANALÝZA ZASOLENIA V MIERKE POĽA: POROVNANIE ROZDIELNYCH MODELOVÝCH PRÍSTUPOV

P. J. Vaughan, P.J. Shouse, D.L. Suarez,
M. Th. van Genuchten, J.E. Ayars

Salinizácia pôdy a zaťaženie podzemných vôd soľami je významným potenciálnym problémom poľnohospodárskej produkcie západnej časti San Joaquin Valley, California. Pokúsili sme sa modelovať transport Cl^- vo vrchnej, 3m vrstve pôdy v 45 lokalitách na 65ha polí v San Joaquin Valley, s využitím štandardných možností CDE a alternatívnych MIM opcií programu Unsatchem. Odber vzoriek pôdy v tejto lokalite bol vykonaný v piatich termínoch, počnúc novembrom 1995 a končiac novembrom 1997. Predpovedné možnosti modelu boli vyhodnotené výpočtom SRMSE pre štyri po sebe nasledujúce termíny odberu vzoriek pôdy. Model CDE predpovedal podstatne vyššie vyplavovanie solí, ako bolo v skutočnosti. Tento problém sme riešili zdokonalením modelu pre MIM transport roztokov a zvýšili sme potenciánu intenzitu transpirácie 1,5-krát. Zvýšenie intenzity potenciálnej transpirácie spôsobilo zvýšenie transportu chloridov smerom nahor, čo spôsobilo zníženie mediánu SRMSE pre CDE z 82 na 76 %. Simulácie modelom MIM boli vykonané systematickou variáciou dvoch parametrov modelu MIM (t.j. pomerným podielom imobilnej vody η a súčiniteľom prenosu hmoty ω). Séria simulácií s využitím optimálnych hodnôt týchto parametrov zlepšila predpoveď profilov Cl^- redukciou mediánu SRMSE na 72 %. Pre 64 % lokalít koeficienty prenosu hmoty v rozsahu $10^{-4} \leq \omega \leq 10^{-3}$ spolu s relatívne vy-

sokým podielom imobilnej vody viedli k našim najlepším prognózam.

Modely CDE a MIM boli potom vyhodnotené porovnávaním tvarov predpovedaných a meraných profilov Cl^-. Zistilo sa, že model CDE mal silnú tendenciu predpovedať monotónne klesajúci profil Cl^- pre november 1997. V tom istom čase merané profily chloridov mali rôzne tvary, 31 % z nich malo maximum Cl^- vo vrchných 1,5m vrstvách. MIM predpovedal maximá v 41 % lokalít. Predpovede tvarov profilov s modelom MIM boli podstatne lepšie ako predpovede s použitím CDE. Podstatným nedostatkom modelov MIM bola neschopnosť generovať veľké amplitúdy maxím Cl^-, ktoré boli pozorované v niektorých lokalitách.

Budúce štúdie modelov môžu byť nasmerované na spôsob, ako sú generované a v závlahových podmienkach zachovávané maximá Cl^-, vrátane dôvodu, prečo tieto maximá Cl^- sú priestorovo rozložené. Táto štúdia tiež ukázala, aké je dôležité presné určenie intenzity evapotranspirácie. Napríklad, kontinuálne meranie intenzity evapotranspirácie počas poľného experimentu s využitím pulzačnej (eddy covariance) metódy môže viesť k veľmi potrebnému zlepšeniu výsledkov. Potrebný je tiež ďalší výskum dolných okrajových podmienok v pôdach so systematickou rúrkovou drenážou v podmienkach neustáleného pohybu hladiny vody.

Zoznam symbolov

b – exponent vo funkcii vodného stresu [–],
c_k – koncentrácia k-tej zložky v pôdnom roztoku [M L^{-3}],
$\bar{c}_k$ – koncentrácia k-tej zložky v substráte na povrchu [M M^{-1}],
$\hat{c}_k$ – koncentrácia k-tej zložky v pevnej fáze [M M^{-1}],
CV – koeficient variácie [–],
D – disperzný koeficient [L^2 T^{-1}],
D_m – koeficient molekulárnej difúzie vo vode [L^2 T^{-1}],
h – tlaková výška vody [L],
h_{crit} – minimálna hodnota tlakovej výšky vody na povrchu pôdy [L],
h_ϕ – osmotická tlaková výška [L],
h_{50} – tlaková výška vody pri 50% redukcii stresom [L],
$h_{\phi 50}$ – osmotická tlaková výška pri 50% redukcii stresom [L],
O_i – pozorovaná koncentrácia Cl^- [M L^{-3}],
P_i – modelom predpovedaná koncentrácia Cl^- [M L^{-3}],
q – intenzita toku vody [L T^{-1}],
S_p – potenciálna intenzita rozdelenia odberu vody koreňmi [L^3 L^{-3} T^{-1}],
$SRMSE$ – relatívna hodnota kvadratickej odchýlky [–],
t – čas [T],
z – vertikálna súradnica [L],
α_s – funkcia závislá na vodnom strese [–],
α_ϕ – funkcia závislá na osmotickom strese [–],
η – koeficient pre pre podiel "nepohyblivej" vody v pôde [–],
θ_w – objemová vlhkosť pôdy [–],
θ_r – reziduálny obsah vody [–],
θ_s – vlhkosť vodou nasýtenej pôdy [–],
θ_m – vlhkosť „pohyblivej" časti vody v pôde [–],
θ_{im} – vlhkosť „nepohyblivej" časti vody v pôde [–],
λ – disperzivita [L],
ρ – objemová hmotnosť pôdy [M L^{-3}],
η – relatívna vlhkosť „nepohyblivej" vody v pôde [–],
τ_w – tortuozita [–],
ω – koeficient prenosu hmoty [T^{-1}].